Orozco-Arboleda, LM.; Renz, M.; Corma Canós, A. (2017). Cerium oxide as catalyst for the ketonization of aldehydes:
Mechanistic insights and a convenient way to alkanes without
consumption of external hydrogen. Green Chemistry. 19(6):1555-1569.
doi:10.1039/C6GC03511F

Green Chemistry

Accepted Manuscript

ROYAL SOCIETY OF CHEMISTRY

rsc.li/green-chem

View Article Online
DOI: 10.1039/C6GC03511F

Green Chemistry

ARTICLE

Cerium oxide as catalyst for the ketonization of aldehydes: Mechanistic insights and a convenient way to alkanes without consumption of external hydrogen

Received 00th January 20xx,
Accepted 00th January 20xx

DOI: 10.1039/x0xx00000x

www.rsc.org/

Lina M. Orozco,[a] Michael Renz*[a] and Avelino Corma*[a]

The ketonization of aldehydes joins two molecules, with n carbon atoms each, to a ketone with 2n–1 carbon atoms. When employing cerium oxide as catalyst with nano-sized crystals (<15 nm) the ketone can be obtained in almost 80% yield. In addition, other ketones are observed so that the total ketone selectivity reached almost 90%. Water is consumed during the reaction when the aldehyde is oxidized to the corresponding carboxylic acid, which is established as a reaction intermediate, co-producing hydrogen. Consequently, water has to be co-fed in the reaction to enhance reaction rate and to improve catalyst stability with time on stream. In contrast to zirconium oxide which possesses catalytic activity for the aldol condensation liberating water, with cerium oxide water is not abundant on the surface and the reaction kinetics show that the reaction rate depends on the concentration of the water in the gas-phase, in addition to the dependence on the gas-phase concentration of the aldehyde. The liberated hydrogen can be consumed in the hydrodeoxygenation of the ketone product. Doing so, when starting from heptanal, a biomass derived aldehyde, an alkane mixture was obtained with almost 90% diesel content. For the whole cascade reaction with five single steps no reagents are necessary and the only by-product is one molecule of innocuous carbon dioxide (related to two molecules of aldehyde). This shows that cerium oxide possesses a big potential to convert biomass derived aldehydes into biofuels in a very sustainable way.

Introduction

The formation of carbon-carbon bonds is an interesting task in chemistry and in biomass conversion. Non-edible biomass consists mainly of lignocellulose which is a composite material out of three biopolymers: cellulose, hemicellulose and lignin. The former are built up by acetal linkages which can be hydrolysed relatively easily so that the monomers are accessible from this feedstock. These monomers consist of monosaccharides with five or six carbon atoms. This is a small number of carbon atoms for a number of chemical products and fuels and, consequently, two or more molecules have to be joined.

For the formation of larger molecules with a low oxygen content from monosaccharides, two strategies can be applied: a complete hydrodeoxygenation to oxygen-free olefins with subsequent oligomerization[1,2] or partial deoxygenation followed by more selective transformations. The latter can be achieved with molecules with simple oxygen functionalities, such as alcohols, aldehydes, ketones or carboxylic acid derivatives. Manifold carbon-carbon forming reactions are known for these compounds as e.g. the Guerbet reaction,[3,4] the aldol condensation of carbonyl compounds,[5,6] the Claisen condensation of esters,[7,8] the ketonic decarboxylation of carboxylic acids,[9] and many others. On the other hand, the first option, i.e. initial hydrodeoxygenation, is mainly applied for fuel production.

Among the reactions for oxygen-containing molecules, the ketonization of aldehydes is a less classical pathway for the formation of carbon-carbon bonds (eq. 1). Aldehydes are a class of organic compounds abundant in biomass derived mixtures such as bio-oils or similar.[10–15] In this reaction, two molecules of aldehyde are transformed into a symmetrical ketone and an oxygenated C_1 fragment, carbon monoxide or carbon dioxide. Although the reaction is carried out at high temperature (> 400 °C), many demands of Sustainable Chemistry are met as e.g. the use of a catalyst and the absence of a solvent or further reactants which minimizes wastes. As an additional benefit of the reaction, the energy, which in general is wasted when an aldehyde is oxidized to its corresponding carboxylic acid employing a sacrificial oxidant, can be recovered in form of hydrogen during the ketonization reaction. Recently, we have shown that the reaction proceeds in two steps when employing zirconium oxide as catalyst.[16] First the aldehyde is oxidized to the corresponding carboxylic acid (eq. 2) which is then transformed into the ketone via the classic ketonic decarboxylation (eq. 3).

[a] Instituto de Tecnología Química, Universitat Politècnica de Valencia-Consejo Superior de Investigaciones Científicas (UPV - CSIC), Av. de los Naranjos s/n, E-46022 Valencia, Spain. Tel.: +34 96 387 7800, Fax: +34 96 387 9444, acorma@itq.upv.es, mrenz@itq.upv.es

Electronic Supplementary Information (ESI) available: further experimental and analytical details, HRTEM images of nanocrystals of CeO_2, details on the kinetic data, the distribution of alkanes produced in the cascade reaction and the McLafferty rearrangement of 7-tridecanone to produce 2-octanone. See DOI: 10.1039/x0xx00000x

View Article Online DOI: 10.1039/C6GC03515F

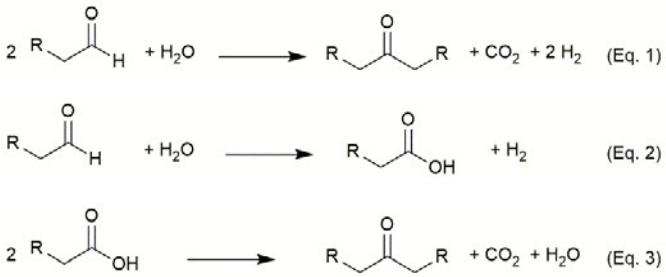

Interestingly, the oxidation proceeds consuming water which provides the necessary oxygen atom and a proton. In a surface-assisted reaction an aldehyde-hydrate species is formed and this species is able to transfer a hydride species to the surface (Scheme 1). Combination of the latter with a proton liberates molecular hydrogen. The carboxylic acid can then react with a second molecule following the established mechanism,[17] forming the carbon-carbon bond between a double-deprotonated and a dehydroxylated species. This intermediate releases carbon dioxide and forms the final ketone product.

This mechanism has been established for the reaction with zirconium oxide and the question which has to be still addressed is if this mechanism applies in general for all catalysts or if it changes for other catalytic materials. Therefore, herein an alternative material, namely cerium oxide, has been chosen to see if the mechanism is the same for both oxides, and how different surface properties of cerium oxide can influence catalytic results. One fundamental difference between zirconium oxide and cerium oxide is that the former is a non-reducible material whereas in the latter the metal oxide possesses redox-properties and the metal atoms can change their oxidation state between plus three and plus four. In addition, catalytic activity induced by surface properties is different. For instance, zirconium oxide facilitates aldol condensation (with water as side product) whereas cerium oxide does so in a less pronounced way.[18] As a consequence, a better selectivity for the ketonization reaction over cerium oxide might be expected due to a lower consumption of the aldehyde in side-reaction pathways, but also the "water supply", required for the aldehyde ketonization and provided by aldol condensation, might be critical.

When the alkanes are the desired products the ketone product can be completely hydrodeoxygenated by a hydrogenation-dehydration-hydrogenation sequence which is carried out over a supported metal in combination with a weakly acidic support. When considering the whole sequence from the two aldehyde molecules (eq. 4), this reaction cascade resembles olefinations of aldehydes following the Wittig, Peterson or Tebbe procedure[19] with subsequent double bond hydrogenation and with the particularity that the carbon chain length is shortened by one carbon atom. As the addition of sophisticated reagents is not required, the atom efficiency is much better on the expense of the loss of one carbon atom as carbon dioxide. Therefore, the combination of these two reaction sequences will be studied here with the aim to confirm that this cascade reaction provides a useful alternative for the direct conversion of aldehydes into alkanes.

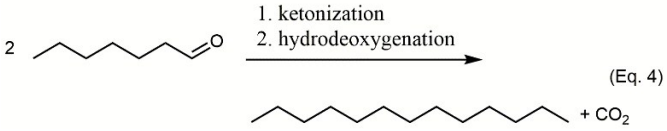

Experimental

General

Heptanal and heptanoic acid were purchased from Sigma-Aldrich and heptanal distilled under reduced pressure before being used. Water was employed in deionized form. Cerium oxide (CeO_2-6nm and CeO_2-11nm) were received from Rhodia or purchased from Aldrich (CeO_2-43nm) as a powder. *m*-ZrO_2 and Al_2O_3 were purchased from Chempur as pellets. Chloroplatinic acid hydrate ($H_2PtCl_6 \cdot 6H_2O$), Sodium borohydride ($NaBH_4$) and 5% Palladium on activated charcoal (5% Pd/C) were bought from Aldrich.

Scheme 1. Proposed mechanism for the ketonization of aldehydes. An aldehyde molecule coordinates to a surface hydroxyl group changing the geometry at the carbonyl carbon atom from trigonal planar to tetrahedral. In the latter configuration it is proposed that a hydride species is shifted to the surface which then combines with a proton and desorbs as molecular hydrogen. The remaining carboxylate can then react via the established mechanism, after a second deprotonation, with a second carboxylic acid molecule. The latter is activated by dehydroxylation and the carbon-carbon bond is formed by a nucleophilic attack onto this carbonyl carbon atom. The formed beta-ketoacid is decarboxylated and the products, ketone and carbon dioxide, are desorbed and the surface hydroxyl group restored by adsorption of one molecule of water.[16]

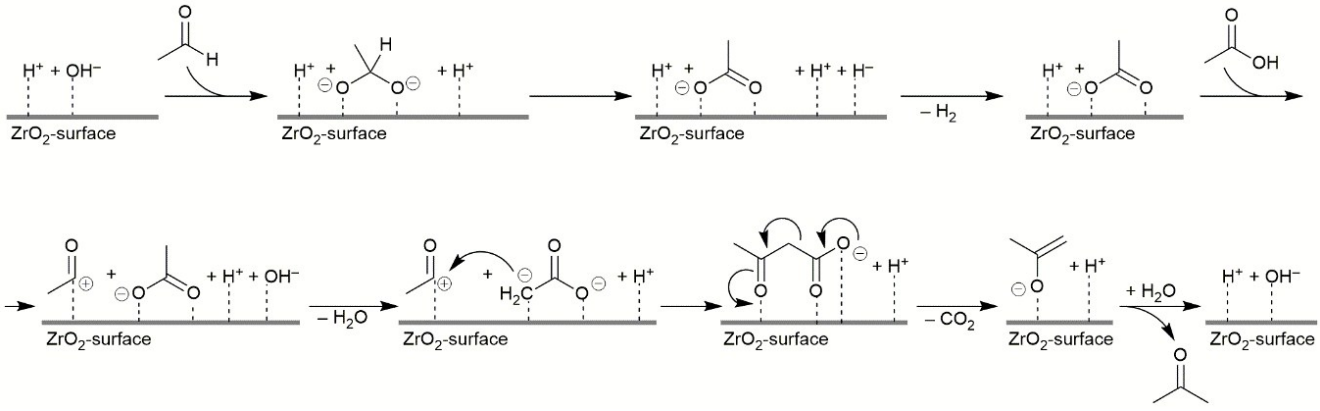

View Article Online
DOI: 10.1039/C6GC03515E

CeO_2 synthesis with different particle size

$Ce(NO_3)_3 \cdot 6H_2O$ was used as the cerium source to obtain CeO_2 nanoparticles following a literature procedure.[20] To get CeO_2-5nm and CeO_2-7nm, $Ce(NO_3)_3 \cdot 6H_2O$ (13.4 g) and NaOH (221.6 g) were dissolved in 76 and 540 mL of deionized water, respectively. The two solutions were mixed and stirred for 30 min forming a milky slurry. Subsequently, the mixture was placed in a 1-L glass bottle and sealed tightly. Finally, the bottle was heated statically in an oven to 100 °C for 24 h. After the hydrothermal treatment, a fresh white precipitate was separated by filtration, washed several times with deionized water until neutral pH, dried at 100 °C in air overnight and calcined at 450 °C for 4 h. Yellow powders (5.3 g, and 5.4 g respectively, 40% yield) were obtained after calcination. To get CeO_2-12nm, the same procedure was employed but the mixture was prepared using different quantities of the reagent: $Ce(NO_3)_3 \cdot 6H_2O$ (3.34 g) and NaOH (55.4 g), which were dissolved in 19 and 135 mL of deionized water, respectively. The reaction was carried out in a teflon-lined stainless steel autoclave following the procedure mentioned before (1.2 g, 36% yield). The latter procedure was also applied to get CeO_2-29nm and CeO_2-277nm but the hydrothermal treatment was done at 150 °C and 200 °C, respectively. In the case of the CeO_2-29nm synthesis, 0.062 g NaOH was used and 0.36 g of solid obtained (11% yield). CeO_2-277nm was produced in 29% yield (0.96 g).

The CeO_2-11nm-400min was recovered from the ketonization reactor after reaction in the absence of water for 400 min of time on stream with a low final catalytic activity indicated by a conversion of only 2%. CeO_2-11nm-700min was employed co-feeding water for 700 min of time on stream (77% final conversion).

2% Pt/Al_2O_3 synthesis

The metal catalyst was prepared by incipient wetness impregnation using an aqueous solution of a platinum precursor ($H_2PtCl_6 \cdot 6H_2O$) and Al_2O_3 (pellets 0.4 – 0.8 mm). The solution was prepared dissolving $H_2PtCl_6 \cdot 6H_2O$ (0.081 g, 0.0002 mol Pt) in water (1.6 mL) to impregnate the metal oxide support Al_2O_3 (1.5 g). The catalyst prepared was dried overnight in an oven at 100 °C and reduced *in-situ*.

Catalyst characterization

The as-prepared and commercial cerium oxide catalysts were characterized by X-ray diffraction (XRD) to confirm crystallinity of the active phases and to measure the average particle size. Analyses were performed on a PANalytical CUBIX-PRO diffractometer equipped with a PW3050 goniometer (Cu Kα radiation) provided with a variable divergence slit. High-resolution transmission electron microscopy (HRTEM JEOL JEM-2100F) was used to verify the particle size of the CeO_2-5nm, CeO_2-6nm and CeO_2-11nm catalysts. The Brunauer–Emmett–Teller (BET) analysis was performed using a Micromeritics ASAP 2420 analyser with a nitrogen bath. Catalysts were out-gassed at 200 °C in vacuum prior to the analysis until the static pressure remained lower than 70 Pa. The ceria catalysts were examined using N_2 adsorption and the BET method was used to calculate the surface area in the range of relative pressures between 1 and 20 Pa. Temperature programmed reduction (TPR) for ceria catalysts was carried out on a conventional flow apparatus (Autochem 2910, Micromeritics). A 0.3-g sample was pretreated in an O_2 (2%)/He flow at 550 °C for 1 h and cooled in a He flow to room temperature, followed by Ar purge. The sample was then reduced in a H_2 (10%)/Ar flow. Temperature was increased from room temperature to 950 °C at a constant heating rate of 10 $K \cdot min^{-1}$ and held for 5 min. Water produced during the reduction was eliminated with a frozen *n*-propanol trap and the amount of consumed H_2 was monitored by a thermal conductivity detector (TCD). The FTIR measurement on the catalyst CeO_2-11nm was performed with a Nicolet iS10 spectrometer from Thermo Fisher equipped with a DTGS detector using a vacuum cell (4 cm^{-1}, 32 scans). The catalyst was employed as self-supported wafers of 1 cm diameter and 22 mg weight. For the D_2O adsorption experiments the catalyst was treated for 1.5 h at 120 °C and 1 h at 450 °C under vacuum ($8.6 \cdot 10^{-2}$ Pa). After activation, the sample was cooled down to room temperature followed by D_2O dosing (1.55 mL gas volume) at increasing pressures (260–530 Pa) until surface saturation, indicated by physisorption, and the IR spectrum recorded after each dose. The active site strength was measured by water evacuation at $8.6 \cdot 10^{-2}$ Pa at room temperature, 150, 350 and 450 °C, recording an IR spectrum after each evacuation. For the thermal gravimetric (TG) analysis, a Mettler Toledo TGA/SDTD 851e was utilized in a 50–900 °C temperature range and a ramp of 10 $K \cdot min^{-1}$ under an air flow of 35 $mL \cdot min^{-1}$. ^1H and ^{13}C NMR experiments were performed on a Bruker 300 / 54 mm Ultrashield (300 MHz for ^1H and 75 MHz for ^{13}C). ^1H and ^{13}C chemical shifts are reported in ppm *versus* $Si(CH_3)_4$ (TMS).

Catalytic tests in a fixed-bed, continuous-flow reactor

Transformations of heptanal and alternative reactions (hexanoic acid-heptanal, hexanoic acid-heptanoic acid, heptanoic acid-nonanoic acid and aldol condensation product 2-pentyl-2-nonenal) were carried out in a tubular stainless-steel reactor. The ceria catalysts (1.0 g, pellets, 0.2 – 0.4 mm) were diluted with silicon carbide (2.0 g), placed as a fixed bed in a stainless-steel tube (0.4 cm internal diameter and 20 cm length) and calcined at 450 °C for 2 h in air (100 $mL \cdot min^{-1}$). The reactor was heated to 450 °C under ambient pressure. Heptanal (5 mL) was reacted at 0.2 $mL \cdot min^{-1}$ under N_2 flow of 198 $mL \cdot min^{-1}$ or feeding heptanal-water molar ratio of 1 to 1 (0.026 $mL \cdot min^{-1}$ water, 163 $mL \cdot min^{-1}$ N_2) with CeO_2-6nm and CeO_2-11nm. For CeO_2-5nm, CeO_2-7nm and CeO_2-12nm, heptanal was reacted feeding 0.1 $mL \cdot min^{-1}$ with a N_2 flow of 98 $mL \cdot min^{-1}$ or feeding heptanal-water with a molar ratio of 1 to 1 (0.013 $mL \cdot min^{-1}$ water, 80 $mL \cdot min^{-1}$ N_2). 2-pentyl-2-nonenal (0.147 $mL \cdot min^{-1}$) and water (0.0847 $mL \cdot min^{-1}$) were fed separately into the reactor with molar ratio of 1 : 8 together with a nitrogen flow of 29 $mL \cdot min^{-1}$ employing CeO_2-6nm as catalyst. The reaction mixtures mentioned before were passed through the reactor at 450 °C, with a flow rate of 0.147 $mL \cdot min^{-1}$ together with a N_2 flow of 144 $mL \cdot min^{-1}$ for heptanoic acid-nonanoic acid (over *m*-ZrO_2) and, for the other mixtures, with a N_2 flow of 122 $mL \cdot min^{-1}$ and water of 0.02 $mL \cdot min^{-1}$ using CeO_2-11nm.

The liquid product was condensed with an ice bath at the exit of the reactor and analyzed offline by GC with an Agilent 7890A apparatus, equipped with a HP-5 column (30 m, 0.32 mm, 0.25 µm) and a FID detector, using *n*-dodecane (Aldrich) as an external standard. Gaseous products were trapped in a gas burette and analyzed by GC on a Varian 450 with a "refinery gas analyser" configuration with three channels. Hydrogen was analyzed after separation on a 2 m molecular sieve 5 Å column by a thermal conductivity detector. Permanent gases such as CO and CO_2 were separated on a 2.5 m molecular sieve 13X column and quantified by a thermal conductivity detector. Low molecular weight hydrocarbons were separated on a 50 m Plot/Al_2O_3 column and quantified with a flame ionization detector.

For testing the catalyst stability in the presence and in the absence of water, 65 g of heptanal were fed into the reactor (1 g CeO_2-11nm) until complete catalyst deactivation. With a fresh catalyst bed (1 g CeO_2-11nm) 109 g of heptanal were fed into the reactor with heptanal-water molar ratio 1 : 1, at 450 °C without intermediate catalyst calcinations. Liquid and gas phases were analyzed by GC as mentioned above.

Kinetic measurements of initial rates in a fixed-bed, continuous-flow reactor.

Kinetic measurements were carried out in a tubular stainless-steel reactor at 450 °C and ambient pressure using 0.2 – 0.4 mm pellets of CeO_2-6nm. Adequate N_2 and heptanal flow rates and catalyst particle size were selected to avoid heat and mass transfer limitations. With the aim to determine the kinetic expression of the reaction, initial rates of formation of the principal product (7-tridecanone) were calculated by keeping heptanal partial pressure, water partial pressures and total flow constant while the contact time (W/F) was varied by employing different amounts of catalyst. Heptanal conversions were not higher than 12 %.

Initial rates were calculated for different partial pressures feeding 5 mL of heptanal with partial pressures of 1.5, 3.0, 4.5 and $6.0 \cdot 10^4$ Pa, using heptanal flows of 0.147, 0.293, 0.440 and 0.587 mL·min^{-1} and N_2 flows of 118, 93, 68 and 42 mL·min^{-1} respectively. For each heptanal partial pressure 10, 25 and 40 mg of CeO_2-6nm were used. Water partial pressure of $1.5 \cdot 10^4$ Pa was maintained constant using water flow of 0.019 mL·min^{-1}.

To test the initial rate effect of adding water to the reaction, heptanal partial pressure of $1.5 \cdot 10^4$ Pa was maintained constant using heptanal flow of 0.147 mL·min^{-1}, while heptanal : water molar ratio was varied from 1 : 0, 1 : 0.1, 1 : 0.3, 1 : 0.5, 1 : 1 to 1 : 2 and 1 : 3. Kinetic modelling to fit the experimental data with the proposed rate expression was carried out using the Origin program (Non-linear fit, Levenberg-Marquardt iteration algorithm, coefficient of determination $R^2 = 0.998$).

The activation energy for the heptanoic acid reaction was determined in the absence of water using a heptanoic acid flow of 0.147 and a N_2 flow of 144 mL·min^{-1}, and in the presence of water using a water-heptanoic acid molar ratio of 1 : 1 with a heptanoic acid flow of 0.147 mL·min^{-1}, a water flow of 0. 019 mL·min^{-1} and a N_2 flow of 118 mL·min^{-1}, $1.5 \cdot 10^4$ Pa heptanoic acid partial pressure in the temperature range of 390 to 450 °C employing 25 mg of CeO_2-11nm. The activation energy for the heptanal reaction was determined in the presence of water using a water-heptanal molar ratio of 1 : 1 with a heptanal flow of 0.147 mL·min^{-1}, a water flow of 0. 019 mL·min^{-1} and a N_2 flow of 118 mL·min^{-1}, $1.5 \cdot 10^4$ Pa heptanal partial pressure in the temperature range from 390 to 450 °C employing 25 mg of CeO_2-11nm.

Coupling of heptanal ketonization and 7-tridecanone hydrodeoxygenation carried out in two catalytic beds

The catalysts (CeO_2-11-nm and Pt/Al_2O_3) were placed separately as fixed beds in two connected stainless steel tubular reactors (length of 20 cm and i.d. of 0.4 cm for each one). CeO_2-11-nm (1.0 g, pellets 0.4 – 0.8 mm) and 2 % Pt/Al_2O_3 (1.5 g, pellets 0.4 – 0.8 mm) were packed with 2.0 g and 1.0 g of silicon carbide, respectively. The Pt-containing catalyst was reduced *in-situ* in the fixed-bed continuous-flow reactor.

The catalytic reactions were carried out at a total hydrogen pressure of $2 \cdot 10^6$ Pa controlled by a back-pressure regulator. The first reactor packed with CeO_2-11-nm was heated to 450 °C and the second one filled with 2 % Pt/Al_2O_3 was heated to 300 °C. After catalyst reduction, heptanal (5 mL, 0.1 mL·min^{-1}) and water (0.638 mL, 0.013 mL·min^{-1}) were fed separately into the reactor with a molar ratio of 1 : 1 together applying a hydrogen flow of 220 mL·min^{-1} at a total pressure of $2 \cdot 10^6$ Pa. At the exit of the reactor the liquid product was condensed at 0°C with an ice bath and analyzed off-line by GC y GC-MS. Gaseous products were trapped in a gas burette and analyzed by GC on a Varian 450 with a "refinery gas analysers" configuration with three channels as mentioned above. A simulated distillation was carried out on a Varian 3800-GC chromatograph according to the ASTM-2887-D86 procedure, which is suitable for the distillation of crude oil components boiling at temperatures lower than 400 °C.

Results and discussion

Characterization of the materials

In the present work several cerium oxide materials were employed involving different particle sizes, pore diameters and surface areas. CeO_2-6nm, CeO_2-11nm and CeO_2-43nm were industrial/commercial catalysts, and CeO_2-5nm, CeO_2-7nm, CeO_2-12nm, CeO_2-29nm and CeO_2-277nm were synthesized by hydrothermal treatment at different temperatures. The average particle size was estimated by X-ray powder diffraction (XRD) by means of the Debye-Scherrer equation and the value included into the sample name: CeO_2-xxnm (Table 1). For selected samples the crystal size was verified by high-resolution transmission electron microscopy (HRTEM, Figure S1).

The BET surface areas of the samples, measured by nitrogen adsorption, varied from 19 to 234 m^2·g^{-1}, but were not in line with the particle size. The CeO_2-6nm sample possessed a much higher surface area than the synthesized ones, e.g. CeO_2-5nm, with values of 234 and 174 m^2·g^{-1}, respectively (Table 1, entries 1 and 2). Also the average pore size of the two industrial samples, CeO_2-6nm and CeO_2-11nm, were different from the

View Article Online
DOI: 10.1039/C6GC03511F

Table 1. Physical and textural properties of the cerium oxide materials.

Entry	Catalyst	S_{BET}[a] [$m^2\ g^{-1}$]	D_p[b] [Å]	V_p[c] [$cm^3\ g^{-1}$]	Reducible sites[d] [wt% (°C)]	Crystal size[e] [nm]
1	CeO_2-5nm	174	64	0.22	n.d.	5
2	CeO_2-6nm	234	31	0.10	35 (465); 32 (747)	6
3	CeO_2-7nm	138	79	0.23	n.d.	7
4	CeO_2-11nm	114	47	0.15	17 (452); 17 (769)	11
5	CeO_2-12nm	110	66	0.14	n.d.	12
6	CeO_2-29nm	33	87	0.05	18 (477); 21 (712)	29
7	CeO_2-43nm	47	95	0.10	15 (387); 28 (750)	43
8	CeO_2-277nm	19	114	0.04	9 (392); 24 (713)	277
9	CeO_2-11nm-400min[f]	106	50	0.15	n.d.	11
10	CeO_2-11nm-700min[g]	92	54	0.14	n.d.	12

[a] Specific surface area calculated by the BET method using N_2 adsorption isotherm at −196 °C. [b] Average BJH pore size. [c] Average BJH pore volume. [d] From Temperature-Programmed Reduction (TPR) measurements, see also Figure 2. [e] From X-ray measurements: the particle size determination was done using the Debye-Scherrer equation for particles of spherical shape.[44] [f] Catalyst used in the absence of water for 400 min; area measurement after calcination. [g] Catalyst used in the presence of water for 700 min; area measurement after calcination.

synthesized materials with 31 and 47 Å, respectively (Table 1, entries 2 and 4). All other samples had much larger average pore diameters (from 64 to 114 Å; Table 1, entries 1, 3 and 5 to 8). The XRD patterns of all CeO_2 samples corresponded to the *cubic* phase of fluorite, in which Ce has a cubic eight-fold coordination to oxygen[21] (Figure 1).

The redox properties were all similar and TPR curves of selected samples are shown in Figure 2. Reduction occurred in two temperature ranges: a low temperature region (300–550 °C) with a maximum at around 470 °C attributed to the surface reduction of the Ce^{4+} ions, and a high temperature region (600–900 °C) with a maximum at around 750 °C, probably related to the reduction of the bulk oxide.[18] With decreasing BET surface area, the area of the peak in the higher temperature region (indicating bulk reduction) becomes bigger with respect to the one in the lower temperature region (Table 1) which is in accordance with the interpretation of surface reduction *versus* bulk reduction of the respective temperature regions.

In order to gain insight into the hydroxylation (hydration) process of the CeO_2–surface an *in-situ* FTIR-study was carried out on the CeO_2-11nm sample with deuterated water. The sample was calcined at 450 °C during 60 min prior to the treatment with D_2O and IR spectra were recorded at room temperature before and after introducing repeatedly small determined amounts of D_2O gas into the cell. Finally, pressure was equilibrated at 227 Pa with D_2O vapour, excess water was removed again by applying high vacuum at room temperature and then desorbed successively at increasing temperature (150, 350 and 450 °C).

Selected indicative spectra are shown in Figure 3. Spectrum (a) was obtained after the initial calcination not showing any bands in the region from 2800 to 2550 cm^{-1} corresponding to surface deuteroxyl groups. After saturation of the surface with deuterated water and applying vacuum at room temperature, one main band is observed in spectrum (b) at 2700 cm^{-1} which is maintained after desorption at 150 °C (max. at 2696 cm^{-1}, spectrum (c)). After desorption at 350 and 450 °C, in spectra (d) and (e) the shape of the bands changed and two maxima were observed at 2710 and 2680 cm^{-1}. The band at 2696 cm^{-1} has been attributed to bridging OD groups coordinated to two Ce^{IV}

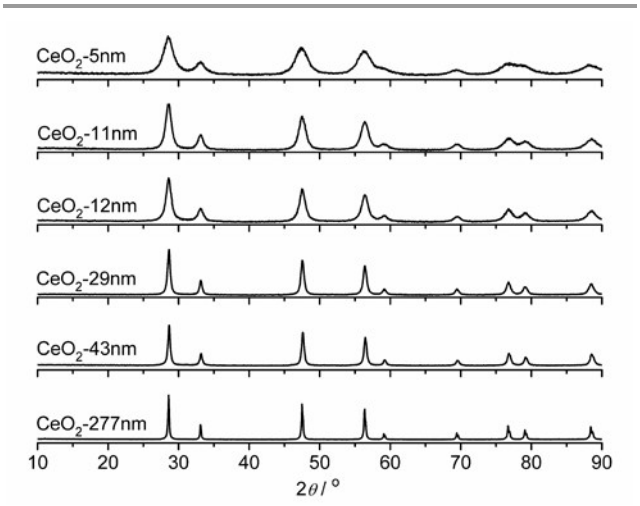

Figure 1. X-ray diffraction patterns of different CeO_2 materials.

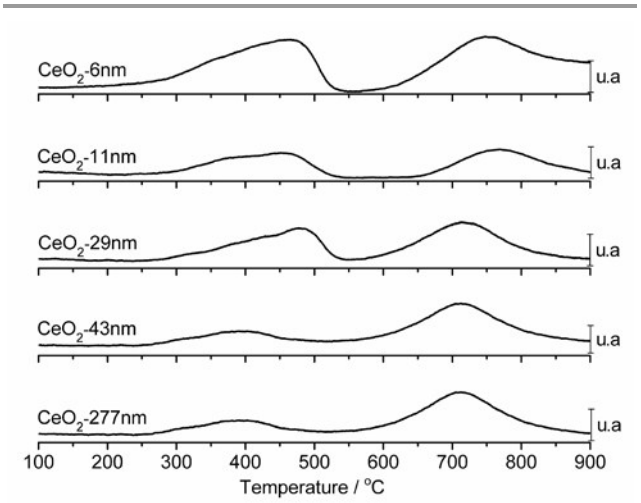

Figure 2. Profiles of the temperature-programmed reduction (TPR) of different CeO_2 catalysts.

View Article Online
DOI: 10.1039/C6GC03515

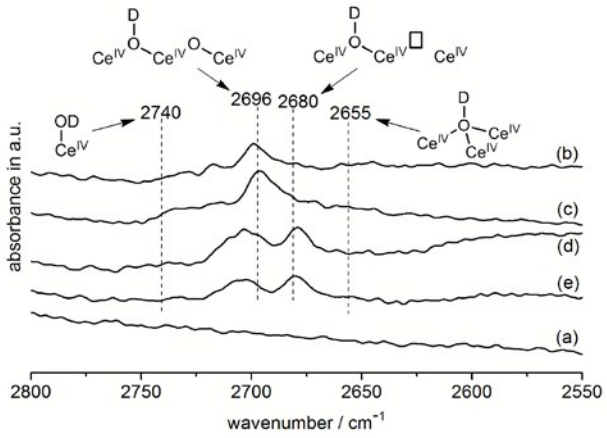

Figure 3. FT-IR spectra for the D_2O adsorption and desorption on CeO_2-11nm. (a) Spectrum after treatment of the sample at 450 °C applying high vacuum ($8.6 \cdot 10^{-3}$ Pa) before D_2O adsorption (non-deuterated OH bands are visible in the 3600 to 3750 cm^{-1} region). (b) Spectrum after saturation of the sample with D_2O and evacuation under high vacuum ($4.6 \cdot 10^{-3}$ Pa) at room temperature, (c) to (e) Spectra after desorption under high vacuum at 150 °C (c), 350 °C (d) and 450 °C (e), respectively.

atoms without any oxygen vacancy in their coordination sphere[22], whereas the band at 2680 cm^{-1} has been assigned to the same doubly coordinated species but with one of the cerium atoms with an oxygen vacancy. Mono-coordinated hydroxy groups (approx. 2740 cm^{-1}) and hydroxy groups shared by three cerium atoms (approx. 2655 cm^{-1}) were not detected in significant quantity.

From the above spectroscopic results it can be concluded that at room temperature the surface is covered by hydroxy groups bridging two cerium atoms. Then when heating up the sample to 350 °C or 450 °C (spectra d and e, respectively), the surface is dehydrated which creates oxygen vacancy evidenced by the presence of hydroxy groups in vicinity of such vacancies (band at 2680 cm^{-1}). In addition, the band for the hydroxy group without adjacent vacancies is shifted to higher wave numbers.

In conclusion, the *in-situ* FTIR study demonstrated that hydroxy groups are present on the CeO_2-surface, even at 450 °C, and that these groups are available for coordination of other molecules, for instance water or aldehyde molecules. Part of the hydroxy groups can be removed by dehydration and oxygen vacancies can be created. Water desorption from the surface is further supported by thermogravimetry (TG) at atmospheric pressure and under air flow. In the region from 400 to 500 °C a weight loss was observed (Figure S2) which was proportional to the BET surface area.

Catalytic results

A screening of the catalysts was performed in a fixed-bed continuous flow reactor aiming to high conversion and high ketone yield. Hence, heptanal was fed in presence (1 : 1 molar ratio) and absence of water at 450 °C (Table 2, entries 4 and 5, respectively). A cerium oxide material with an average crystal size of approximately 11 nm (CeO_2-11nm) was used as catalyst. In both cases conversion was almost complete but in presence of water the selectivity towards the desired ketone, i.e. 7-tridecanone, was higher with 66% *versus* 56%. The selectivity was improved still further by decreasing the average crystal size of the CeO_2 to approximately 6 nm (CeO_2-6nm, Table 2, entry 2). The selectivity towards the desired ketone product was raised to 79% in the presence of water. Apart from the C_{13}-ketone, a series of linear ketones with different carbon atom number was observed (molecular weight distribution and formation will be discussed below) and the selectivity towards all ketones reached almost 90%. The aldol condensation product and products derived from it were observed in total in approx. 5% yield. Whereas the selectivity seems to be related to the crystal size, the catalytic activity indicated by the conversion

Table 2. Heptanal conversion and selectivities over different CeO_2 catalysts for the ketonization of heptanal in the presence of water. Reaction conditions: 1.0 g of catalyst was placed in a fixed bed and heptanal (5 mL, 0.2 mL·min^{-1}) and water (0.026 mL·min^{-1}), molar ratio 1 to 1, were reacted in the gas phase in a continuous-flow reactor at 450 °C under nitrogen flow (163 mL·min^{-1}), heptanal partial pressure $1.5 \cdot 10^4$ Pa, W/F 706 g·min·mol^{-1}.

			Selectivity[a]				
Entry	Catalyst	Conv. [%]	7-$C_{13}H_{26}O$ [%]	Total ketones[b] [%]	Aldol Cond.[c] [%]	Hydrogen. aldol cond.[d] [%]	Others[e] [%]
1	CeO_2-5nm[f]	88.5	77.3	87.7	4.4	0.9	7.0
2	CeO_2-6nm	99.6	78.9	87.8	2.3	0.0	9.9
3	CeO_2-7nm[f]	76.6	74.0	84.1	5.0	1.4	9.5
4	CeO_2-11nm	97.8	66.4	81.6	4.3	1.3	12.8
5	CeO_2-11nm[g]	94.4	56.0	75.5	6.5	4.3	13.7[h]
6	CeO_2-12nm[f]	76.2	69.4	82.0	6.0	1.2	10.8
7	CeO_2-43nm	29.8	57.7	76.5	6.7	0.0	16.8[i]
8	CeO_2-6nm[j]	40.0	12.6	21.8	31.6[k]	31.1	15

[a] Selectivity calculated with respect to the aldehyde substrate taking into account the reaction stoichiometry: two aldehyde molecules form one ketone molecule or one molecule of the other products. [b] Total selectivity of ketones including 7-tridecanone; more detailed information on the distribution of the minor ketones can be obtained from Figure 10. [c] Selectivity of the aldol condensation product, partly isomerized. [d] Saturated aldehyde with molecular formula $C_{14}H_{28}O$, produced by carbon-carbon bond hydrogenation of the aldol condensation product. [e] Other products observed in the liquid phase and quantified by GC. [f] Reaction was carried out with 0.50 g of catalyst, scaling down all reactant and gas flows to W/F stablished. [g] Reaction carried out without co-feeding water. Reaction conditions: heptanal (5 mL, 0.2 mL·min^{-1}) and N_2 (198 mL·min^{-1}): [h] Olefins are observed in 5% selectivity. [i] 1-Heptanol was observed with 12% selectivity. [j] 2-pentyl-2-nonenal (aldol condensation product) employed as feed together with water. Reaction conditions: 1.0 g of CeO_2-6nm was placed in a fixed bed and 2-pentyl-2-nonenal (5 mL, 0.147 mL·min^{-1}) was reacted under nitrogen flow (29 mL·min^{-1}), feeding 2-pentyl-2-nonenal and water with a molar ratio of 1 to 8 (0.085 mL·min^{-1} water); 2-pentyl-2-nonenal partial pressure $1.5 \cdot 10^4$ Pa. [k] Only isomerized aldol-condensation product.

View Article Online
DOI: 10.1039/C6GC03515

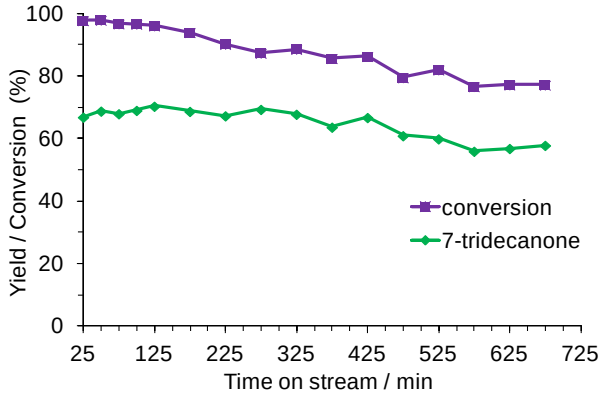

Figure 4. Catalytic performance of CeO_2-11nm with time on stream in the ketonization of heptanal in the presence of water. Reaction conditions: heptanal - water molar ratio 1 : 1, 0.2 mL·min^{-1} heptanal, 0.026 mL·min^{-1} water, 163 mL·min^{-1} N_2 and 450 °C. During the reaction 109 g of heptanal were passed per g of catalyst.

degree is not clearly related to the textural properties such as BET surface area or pore volume for a crystal size < 15 nm (cf. Table 1 and Table 2). The best correlation can be found between average channel size and conversion degree. In any case, raising the crystal size significantly to 43 nm (which implicates a low surface area of the material of 47 m^2 g^{-1}) decreases conversion degree drastically to only 30% under otherwise identical conditions (Table 2, entry 7).

The water had an effect on product selectivity on short term and it had an influence on the catalytic performance at longer term. Whereas the catalyst is fairly stable when co-feeding water (Figure 4), in absence of water a rapid decline of activity was observed (Figure 5). When the latter catalyst was recovered from the reactor, its black colour indicated coke deposition which could be quantified by TG in presence of air to be a 15% of catalyst weight. However, calcination in air could only restore the catalytic activity partly. A conversion of 45% and a total ketone selectivity of 89% was achieved with the recycled material. This indicated that additional deactivation pathways applied to the catalyst or that the coke elimination procedure has to be further optimized. A small decline in the surface area might contribute to the activity decrease after reactivation by calcination (cf. Table 1, entries 9 and 10) whereas a change in the crystalline phase was not detected (Figure S3).

In conclusion the preliminary catalytic experiments indicated that nanocrystalline cerium oxide is an excellent catalyst for the ketonization of aldehydes providing selectivity to ketones up to 90%. This reactivity could be assumed since literature studies on CeO_2-ZrO_2 mixed oxides[18] or on bigger crystals of CeO_2[23,24] indicated a basic catalytic activity for aldehyde ketonization. In analogy to the reaction catalysed by zirconium oxide, water seems to play a crucial role in this reaction and, therefore, the mechanism and the role of water should be compared for both materials.

Confirmation of the carboxylic acid as reaction intermediate

For zirconium oxide it has been established that the ketonization of aldehydes proceeds by aldehyde oxidation and subsequent classical ketonic decarboxylation of the carboxylic acid as explained before.[16] For the cerium oxide case the same mechanism was assumed as working hypothesis and, therefore, the key-control experiments and analysis were carried out with this material. Gaseous effluents were collected at the exit of the reactor and analyzed off-line (see experimental section for more details). Exactly two equivalents of hydrogen were obtained per molecule of ketone (Eq. 5), which supports the stoichiometric dehydrogenation of the aldehyde. It can then be concluded when the stoichiometric equation is balanced that exactly one water molecule is consumed per ketone produced. Thereby, it has to be kept in mind that, actually two molecules of water are consumed per two equivalents of aldehyde, but one of these is produced during the reaction at a later stage. Almost one equivalent of carbon dioxide was observed per ketone produced which is in accordance to the ketonic decarboxylation mechanism of the intermediary carboxylic acids. A possible reason for the slightly lower value with respect to the theoretical one might be that a small part of carbon

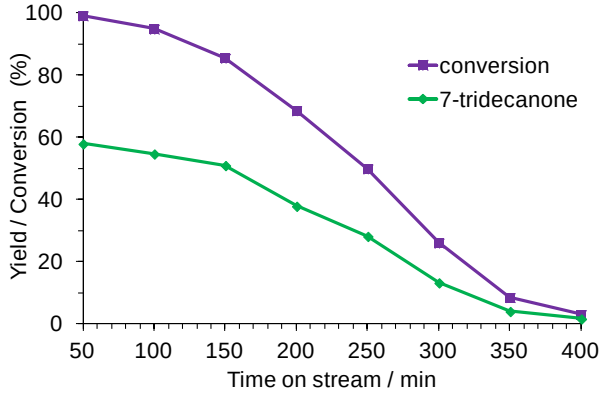

Figure 5. Catalytic performance of CeO_2-11nm with time on stream in the ketonization of heptanal without co-feeding water. Reaction conditions: 0.2 mL·min^{-1} heptanal, 198 mL·min^{-1} N_2 and 450 °C. During the reaction 65 g of heptanal were passed per g of catalyst.

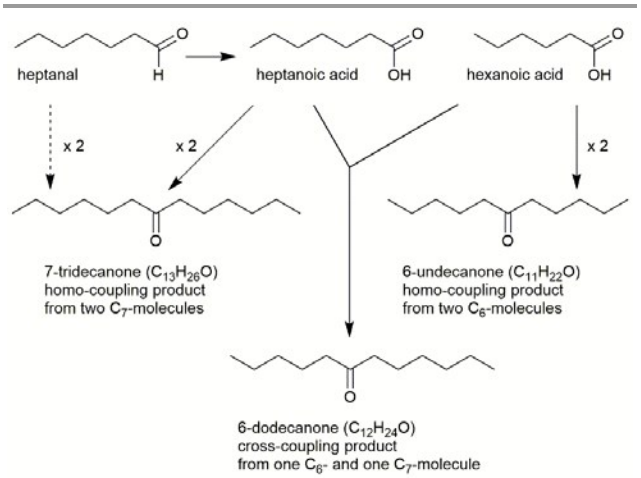

Scheme 2. Schematic description of the cross-coupling experiment between heptanal and hexanoic acid. Cross-coupling product 6-dodecanone can only be obtained if heptanal is oxidized to heptanoic acid during the reaction.

View Article Online
DOI: 10.1039/C6GC03415F

Table 3. Product yields for the cross-coupling product 6-dodecanone and the homo-coupling products 6-undecanone and 7-tridecanone in the reaction of hexanoic acid with either heptanal or heptanoic acid. Reaction conditions: 1.0 g of catalyst was placed in a fixed bed and both reactions were carried out at 450 °C in presence of water with molar ratios of heptanal : hexanoic acid : water = 1 : 1 : 1 and of heptanoic acid : hexanoic acid : water = 1 : 1 : 1, reaction mixture (5 mL, 0.147 mL·min^{-1}), water (0.675 mL, 0.02 mL·min^{-1}), N_2 (122 mL·min^{-1}). Conversion of aldehyde and carboxylic acid was complete in all cases except for entry 2 (94%).

	C7		Product yield		
Entry	substr.	Catalyst	6-undecanone [%]	6-dodecanone [%]	7-tridecanone [%]
1	ald.	*m*-ZrO_2	40	16	22
2	ald.	CeO_2	40	22	26
3	acid	*m*-ZrO_2	25	48	22
4	acid	CeO_2	22	47	24

dioxide is dissolved in the water of the gas burette with which the gas was collected.

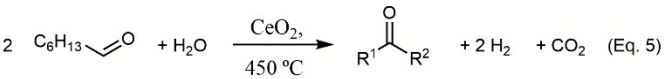

Catalyst:	CeO_2-7nm	Yields/%:	84	84	75
	CeO_2-12nm		82	82	72

The carboxylic acid intermediate should be further confirmed by cross-coupling experiments. If we assume that the carboxylic acid is formed from the aldehyde and it is an intermediate for the global reaction, and then carry out the reaction of heptanal in the presence of other carboxylic acids with different chain length, cross-coupling products have to be produced from the *in-situ* synthesized carboxylic acid and the ones added initially (Scheme 2). Hence, heptanal was reacted with hexanoic acid and, indeed, the corresponding cross-coupling product, i.e. 6-dodecanone, was observed in 22% yield (Table 3). Product distribution between homo-coupling and cross-coupling products was similar for reactions catalysed by CeO_2 and *m*-ZrO_2, but in both cases different from the one observed when reacting both molecules as carboxylic acid. When doing so, the main product is the cross coupling product and the distribution is almost the statistical one of 1 : 2 : 1. The deviation observed when reacting the aldehyde has been explained on the bases of different reaction rates.[16] The second step of the aldehyde ketonization is faster than the first one. As a consequence, carboxylic acid present at an early reaction stage reacts fast to the homo-coupling product and its concentration is decreasing rapidly. In contrast, the aldehyde is converted slowly into the corresponding carboxylic acid which then reacts either with the lower concentrated carboxylic acid or in homo-coupling. This explanation is well in line with the results observed (cf. Table 3). As a consequence, both observations, i.e. the detection of the cross-coupling product and the product distribution, are strong evidences for the carboxylic acid as reaction intermediate from the aldehyde to the ketones.

Alternative mechanisms proposed in the literature for the reaction of aldehydes to the ketone involve the aldol condensation product or adduct as an intermediate.[25–30] If this was the case, the final ketone has to be formed at least as fast from the aldol condensation product as from the aldehyde, and with the same or in better yield. However, when the aldol condensation product is passed over CeO_2 under similar reaction conditions, in presence or absence of water, the ketone is obtained only in 5% yield *versus* 57–79% yield when starting directly with the aldehyde (Table 2, entry 8). This result clearly indicates that the ketone product is not produced directly from the aldol condensation product. Ketones might however be produced by a back shift of the aldol equilibrium from the aldol product to the aldehyde substrates, and then via the corresponding carboxylic acids.

In conclusion, we present two convincing experimental observations that the ketonization proceeds via aldehyde oxidation into the carboxylic acid and not via the aldol condensation product as intermediate.

Kinetics of the reaction and effect of water

In the case of zirconium oxide water has a beneficial effect on the selectivity towards the desired ketone, i.e. 7-tridecanone, but it decreases the reaction rate.[16] Now, the effect of water on the reaction kinetics in the case of cerium oxide should be evaluated. With zirconium oxide and in absence of water the aldol condensation is assumed to provide the water required for the ketonization. For cerium oxide, however, it has been observed before that the catalytic activity for the aldol condensation is much less pronounced and a deficit in water concentration, with respect to the stoichiometric amount necessary for the oxidation reaction, can be expected. Even more, in absence of water a rapid cease of the catalytic activity

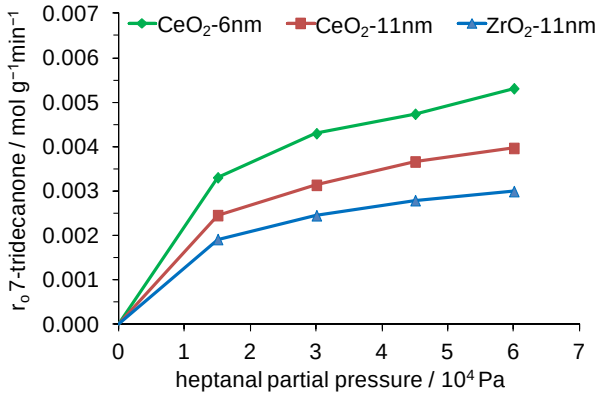

Figure 6. Comparison of experimental initial reaction rates in heptanal ketonization catalysed with CeO_2-6nm, CeO_2-11nm and ZrO_2-11nm in presence of water ($1.5 \cdot 10^4$ Pa) as a function of heptanal partial pressure. Reaction conditions for CeO_2-6nm and CeO_2-11nm: heptanal (5 mL), water (0.019 mL·min^{-1}), catalyst (10, 25, 40 mg), heptanal partial pressure $1.5 \cdot 10^4$ Pa (0.638 mL water, 0.147 mL·min^{-1} heptanal, 118 mL·min^{-1} N_2), $3.0 \cdot 10^4$ Pa (0.319 mL water , 0.293 mL·min^{-1} heptanal, 93 mL·min^{-1} N_2), $4.5 \cdot 10^4$ Pa (0.213 mL water , 0.440 mL·min^{-1} heptanal, 68 mL·min^{-1} N_2), $.6.0 \cdot 10^4$ Pa (0.159 mL water , 0.587 mL·min^{-1} heptanal, 42 mL·min^{-1} N_2). Reaction conditions for ZrO_2-11nm: heptanal (5 mL), water (0.022 mL·min^{-1}), heptanal partial pressure $1.5 \cdot 10^4$ Pa (0.638 mL water, 0.169 mL·min^{-1} heptanal, 6, 15, 23 mg of catalyst, 136 mL·min^{-1} N_2), $3.0 \cdot 10^4$ Pa (0.319 mL water, 0.350 mL·min^{-1} heptanal, 12, 25, 40 mg of catalyst, 110 mL·min^{-1} N_2), $4.5 \cdot 10^4$ Pa (0.213 mL water, 0.518 mL·min^{-1} heptanal, 15, 25, 40 mg of catalyst, 80 mL·min^{-1} N_2) and $6.0 \cdot 10^4$ Pa (0.159 mL water, 0.69 mL·min^{-1} heptanal, 20, 30, 45 mg of catalyst, 50 mL·min^{-1} N_2).

View Article Online
DOI: 10.1039/C6GC03511F

was observed (cf. Figure 5). Therefore, it can be concluded that the kinetics of the reaction in presence of both metal oxides, i.e. *m*-ZrO_2 and CeO_2, have to be different.

The kinetics of the reaction catalysed by cerium oxide was evaluated following the initial-rates methodology. In preliminary experiments it was observed that working at higher heptanal flow than 0.147 mL·min^{-1} and lower catalyst particle size than 0.4 mm the process was not controlled by either external or internal diffusion problems of reactants. At low conversion (<12%) the rate of ketone formation from heptanal was measured, always co-feeding water at a constant partial pressure. When the initial rates of the ketonization with increasing substrate partial pressure are compared for three materials, namely cerium oxide with a crystal size of 6 and 11 nm and a zirconium oxide with a crystal size of 11 nm, it can be seen that the reaction is significantly faster with cerium oxide than with zirconium oxide (Figure 6). In addition, for cerium oxide, the reaction rate is accelerated even more with the smaller crystal-size material. This has to be expected since the material with the smaller crystal size also possesses an increased BET surface area with 234 *versus* 114 m^2 g^{-1} for CeO_2-6nm and CeO_2-11nm, respectively (Table 1, entries 2 and 4), and a higher surface area is generally related to higher catalytic activity. The shape of the kinetic curve, i.e. the dependence on the partial pressure of the aldehyde, is similar in all three cases (Figure 6).

The initial rate was also studied in function of the partial pressure of water in the feed (Figure 7). Interestingly, the figure demonstrates clearly that water is required for the reaction. When the catalyst was freshly calcined to reduce surface hydroxy groups to a minimum (and therewith potential water formation/availability by surface dehydration) and water was not co-fed, the ketone formation rate approached zero. With 0.5 equivalent of water the highest initial rate was achieved and increasing the water amount further the rate decreased again. This effect was more pronounced for the CeO_2-6nm material than for the CeO_2-11nm one.

When co-feeding higher amounts of water, i.e. >0.5 equivalents, a decrease was observed for the ketone formation rate (Figure 7), in a similar manner as for zirconium oxide as catalyst.[16] It has been proposed that competitive adsorption of water to active sites caused this deactivation, impeding an efficient approach of the aldehyde substrate. However, as a clear difference, when the reaction was carried out over zirconium oxide in absence of water (i.e. water partial pressure in the feed = 0) ketone formation was highest. This was related to an efficient water supply by the aldol condensation side reaction which does not occur with cerium oxide, which is much less active than *m*-ZrO_2 for catalysing the aldol condensation. As a consequence, with cerium oxide a certain amount of water has to be added to the feed to achieve the maximum ketone formation rate.

The dependence of the ketone formation on the presence of water in the ketonization of aldehydes over cerium oxide is a clear difference with respect to the zirconium case and this has also to be reflected in the rate equation, although the reaction scheme is the same for both catalysts. In fact, it has been confirmed that the same overall mechanism applies in both cases which is displayed in Scheme 1. Hence, the aldehyde is oxidized in a first step and the corresponding acid converted into the ketone in a second step by a classical ketonic decarboxylation. The carboxylic acid intermediate has been confirmed as such by cross-coupling experiments (Scheme 2) and the hydrogen which has to be produced for the carboxylic acid formation was quantified in the right stoichiometry (Eq. 5). In addition, the aldol condensation product was excluded as intermediate (Table 2, entry 8).

For the zirconium oxide-catalysed reaction the first step, i.e. the aldehyde oxidation, has been identified as rate-determining step (Figure S4) with an activation energy of 198 kJ·mol^{-1}, *versus* 110 kJ·mol^{-1} for the ketonic decarboxylation.[16] When the apparent activation energies were determined over cerium oxide a value of 110 kJ·mol^{-1} (Figure S5) was observed for the

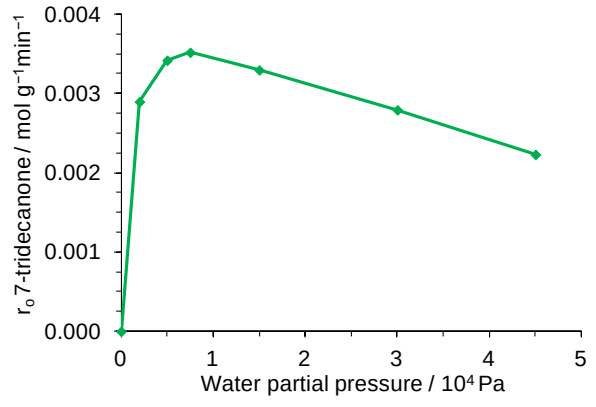

Figure 7. Initial reaction rates in heptanal ketonization catalysed with CeO_2-6nm at heptanal partial pressure of 1.5·10^4 Pa, in the presence of different amounts of water (0.8, 1.5, 3.0 and 4.5·10^4 Pa). Reaction conditions: heptanal (5 mL, 0.147 mL min^{-1}), catalyst (10, 25, 40 mg), heptanal : water molar ratio 1 : 0.5 (0.009 mL min^{-1} water, 130 mL min^{-1} N_2), 1 : 1 (0.019 mL min^{-1} water, 118 mL min^{-1} N_2), 1 : 2 (0.038 mL min^{-1} water, 92 mL min^{-1} N_2) and 1 : 3 (0.056 mL min^{-1} water, 67 mL min^{-1} N_2), 450 °C; without water the reaction was carried out with 144 mL min^{-1} N_2.

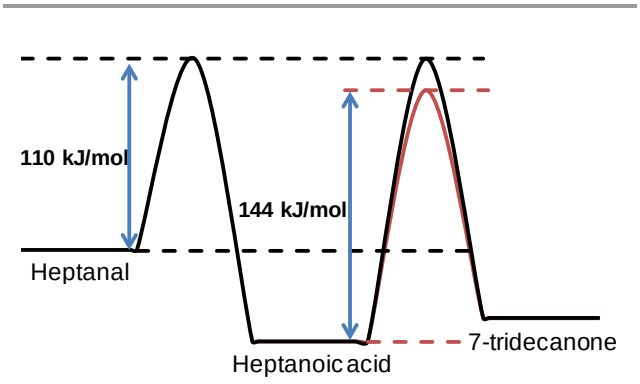

Figure 8. Apparent activation energy for the ketonization of heptanal and of the ketonic decarboxylation of heptanoic acid taking into account the different heat of formation of the organic molecules. The latter values were taken from literature (heptanal[45] and heptanoic acid[46])and the heat of formation of 7-tridecanone from the Cheméo database (https://www.chemeo.com/cid/56-631-9/7-Tridecanone; obtained by the Joback method).[47]

ketonization of heptanal and 144 kJ·mol^{-1} for the ketonic decarboxylation of heptanoic acid in absence of water (Figure S6) and 143 kJ·mol^{-1} in presence of water (1 : 1 molar ratio, Figure S7). Hence, on a first view that activation energy of the second step seemed to be higher than the one of the initial reaction step. However, when the different values for the heat of formation of the molecules were taken into account, the activation step of the first step is still slightly higher than the second one and, therewith, the rate determining step (Figure 8). Also the product distribution of the cross coupling experiment of heptanal and hexanoic acid has been interpreted by means of a faster reaction of the intermediate acid than of the aldehyde. As additional evidence it can be mentioned that heptanoic acid, although being a reaction intermediate, is not accumulated during the reaction but consumed immediately in the second reaction step.

Having identified the rate determining reaction step, all single steps of the reaction were evaluated upon their influence on the reaction rate. As the products formed in the first reaction step, namely carboxylic acid and molecular hydrogen, are the same for both metal oxides, i.e. ZrO_2 and CeO_2, it is assumed that the same intermediates and transition states occur, i.e. the hydrogen is produced from a surface-stabilized aldehyde hydrate (Figure 9, upper right corner). After hydrogen formation the carboxylic acid product has to be desorbed and this step is supposed to be different for the two metal oxides. As on the zirconium oxide surface water is abundant, the carboxylic acid can be replaced directly by a water molecule and the reaction site is ready again for aldehyde adsorption. In contrast, when working with cerium oxide, water is scarcer so that a defect site might be created for a short term which can then be occupied first by an aldehyde molecule or a water molecule. Once both substrates are coordinated, the formation of the surface-stabilized aldehyde hydrate by nucleophilic attack of the hydroxy group to the carbonyl group should be fast again. However, the fact that both molecules have to be incorporated from the gas phase causes a dependence for the concentration of the surface-stabilized aldehyde hydrate on the gas phase concentration for both reagents.

All adsorption and desorption steps of the catalytic cycle on cerium oxide, including the nucleophilic attack of the surface hydroxy group onto the carbonyl group, are fast processes so that the rate-determining step has to be the hydride elimination from the adsorbed aldehyde. The concentration of this species is proportional to the occupancy of the two reaction sites and, therewith, to the gas phase concentrations of both substrates. Consequently, also the overall rate of the reaction depends on their gas phase concentration, and the rate equation should display the water and the aldehyde concentration in the counter:

$$-r_{RCHO} = \frac{a[RCHO][H_2O]}{(1 + b[H_2O] + c[H_2O]^2)(1 + d[RCHO] + e[H_2O])} \quad \text{(Eq. 6)}$$

In the denominator two different centres are reflected, one adsorbing water and the second one the aldehyde. In addition, both centres might be blocked by water. For a detailed derivation of the formula see the ESI.

The rate equation was evaluated employing the data obtained when carrying out the reaction in different conditions at low conversion. Origin software was used to fit equation 6 with the experimental data (Non-linear fit, Levenberg-Marquardt iteration algorithm, coefficient of determination $R^2 = 0.998$; cf. Figure S8 and Figure S9). These results support the proposed kinetic equation and, as a consequence, they confirm the hypothesis that the dehydrogenation of the surface-stabilized aldehyde hydrate is the rate-determining step for the ketonization of aldehydes over cerium oxide.

The reaction network

After having established heptanoic acid as an intermediate for the ketonization of heptanal and the ketonic decarboxylation as second reaction step, the complete reaction network has been worked out to elucidate the formation of the side products. As side products the following compounds were observed: ketones with an alkyl chain length different from the main product, isomerized aldol condensation products and products with a molecular weight of 212 g/mol, which might be derived from hydrogenation of the aldol condensation product.

The ketone side product observed in highest concentration was 2-octanone (Figure 10). From the product distribution it can be assumed that its production should be different from the other ketones as it is the only one with an even number of carbon atoms and its formation can be explained easily. It might be produced by the McLafferty rearrangement from the main product, i.e. 7-tridecanone, as described in Scheme S1. This

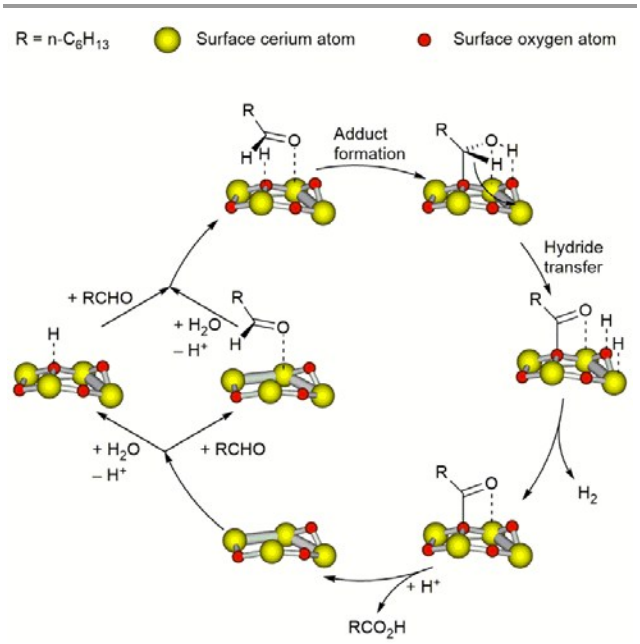

Figure 9. Proposed reaction mechanism for the oxidation of heptanal to heptanoic acid in the presence of CeO_2. At an oxygen vacancy (lower left corner) water and aldehyde are adsorbed in close vicinity to two different sites. One proton from the water is transferred to the oxide surface. Once both substrates adsorbed to the surface, a surface-stabilized analogue of the aldehyde hydrate is formed which then is able to transfer a hydride species to the surface. The latter can combine with a proton and evolve as molecular hydrogen. With a further surface proton (from the initial water adsorption) the carboxylic acid product can be desorbed and the initial free dual site is recovered.

View Article Online
DOI: 10.1039/C6GC03515F

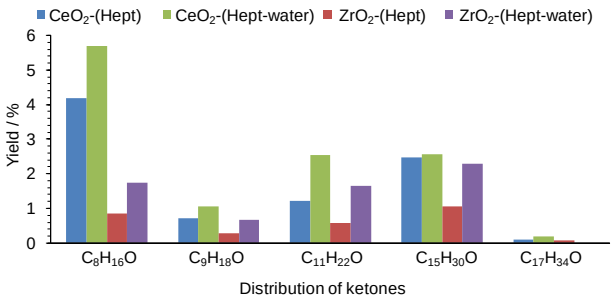

Figure 10. Yields of the different ketone side products in different reactions. $C_8H_{16}O$: 2-octanone; $C_9H_{18}O$: 3-nonanone; $C_{11}H_{22}O$: 5-undecanone; $C_{15}H_{30}O$: 7-pentadecanone; $C_{17}H_{34}O$: 9-heptadecanone.

fragmentation reaction to produce 2-alkanones is typically observed when large chain ketones are produced under severe conditions as for instance by pyrolysis of calcium decanoate.[31] Other ketones were detected and identified by GC-MS, such as e.g. 7-pentadecanone, for which fragmentation was not a possible formation pathway since the number of carbon atoms in this compound was increased with respect to the main product. First of all, the product identification was confirmed unambiguously by comparison with a synthesized authentic sample. Hence, 7-pentadecanone was synthesized by the ketonic decarboxylation of heptanoic and nonanoic acid over zirconium oxide (see ESI). And indeed, mass spectrum and retention time in gas chromatography of the compound detected in the reaction mixture and of the authentic sample were identical. Then, as a working hypothesis it was proposed that the observed product was produced in the same way as the authentic sample was synthesized, i.e. by cross ketonic decarboxylation of nonanoic acid and heptanoic acid. Therefore, nonanoic acid has to be formed under the present reaction conditions.

As a potential source for nonanoic acid the aldol condensation product isomers were identified, which have been detected in the product mixture. It was assumed that the double bond in this molecule can be isomerized on the cerium oxide as depicted in Scheme 3. Acidic and/or basic sites might be responsible for this isomerization. Please notice, the double bond is still in conjugation with the carbonyl group and the formation enthalpy should be similar for both compounds so that thermodynamics favour a statistical distribution for the double bond positions. After shifting back the aldol equilibrium from the isomerized aldol condensation product towards the aldehydes, two molecules of heptanal were converted into one molecule of pentanal and one of nonanal, (Scheme 3) and an alkyl chain length disproportionation had occurred. The corresponding oxidation of the isomerized aldehydes into the carboxylic acids should occur in analogy to the heptanal oxidation. With this reaction sequence of aldol condensation, double bond isomerization and retro-aldol reaction a plausible way to chain-length isomerized aldehydes or carboxylic acids is illustrated.

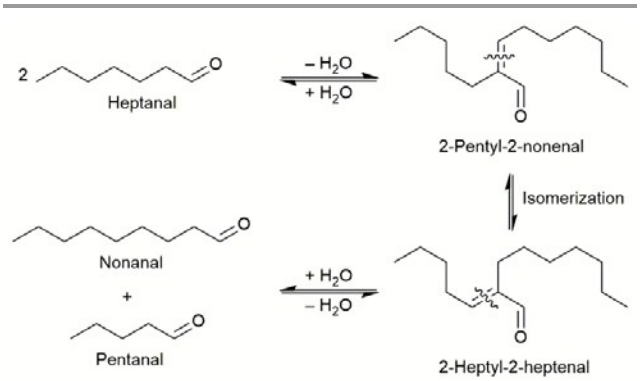

Scheme 3. Proposed mechanism for the chain length isomerization of the aldehyde substrates which is then responsible for the change in the ketone skeleton. Two aldehyde molecules with n carbon atoms form the aldol condensation product. In the latter, the double bond is isomerized into the alternative position, still in conjugation with the carbonyl group. With the retro aldol reaction two different aldehyde molecules are obtained with n+2 and n–2 carbon atoms, respectively.

The chain length isomerization reaction might be understood in analogy to the isomerizing olefin metathesis which leads to regular distributions with a mean chain length.[32] However, to the best of our knowledge this concept has not been reported before for aldehydes. Although in the present case the yield in these chain length isomerization reaction is still low, it is an interesting concept which should be further developed in the future.

If the isomerization occurs as described in Scheme 3, products derived from pentanal should also be detected in the product mixture. Even more, second generation aldehydes such as propanal or products derived from them, might also be observed (in low concentration). Indeed this was the case as the following ketones were detected in the product mixture by GC-MS: 3-nonanone, 5-undecanone, 7-pentadecanone and 9-heptadecanone (Figure 10). These ketones have to be formed from propanal, pentanal, heptanal (the actual starting aldehyde) and nonanal, after having been oxidized to their corresponding acids. This product pattern clearly supports the proposed formation pathway of the ketone side products via isomerization of the aldol condensation product and retro-aldol reaction. A further experimental observation of the present work which also supports this proposed pathway is the increased selectivity towards other ketones (9.2%) with respect to the target compound 7-tridecanone (12.6%), when the aldol condensation product was reacted (Table 2, entry 8) and the

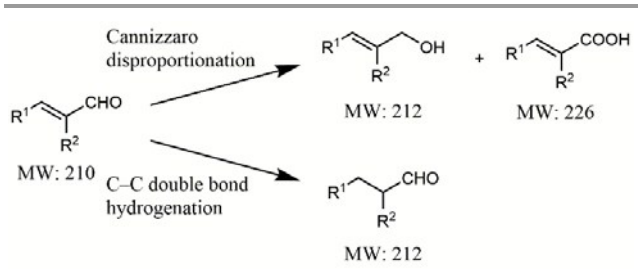

Scheme 4. Proposed mechanisms for the formation of products with a molecular weight of 212 g/mol. The unsaturated alcohol may be produced, together with the unsaturated carboxylic acid, by a Cannizzaro disproportionation. The saturated aldehyde with the same molecular weight may be formed by the C–C double bond hydrogenation.

isomers of the aldol condensation product accounted for 31.6% selectivity.

After having explained the formation of ketone products with different carbon skeleton, the origin of the product with a molecular weight of 212 g·mol^{-1} was examined. This mass corresponds to a hydrogenated aldol condensation product. However, two isomers are possible: the allyl alcohol produced by aldehyde reduction or the saturated aldehyde produced by C–C double bond hydrogenation. As a first hypothesis C–C bond hydrogenation was assumed (Scheme 4, lower pathway). Recently, it has been reported in literature that bare cerium oxide catalyses the hydrogenation of triple bonds.[33,34] In addition, on bare zirconium oxide hydride species have been evidenced during the ketonization of aldehydes[16] and due to the analogy of the mechanism for this reaction on cerium oxide it can be assumed that hydride species are also present on the cerium oxide surface. With the aim to proof this hypothesis the double bond in the aldol condensation product was hydrogenated by molecular hydrogen in the presence of a Pd/C catalyst (Scheme 4, lower pathway). And indeed, GC retention time and the GC-MS mass spectrum confirmed that the product observed in the mixture with a mass of 212 g·mol^{-1} was the double-bond hydrogenated aldol condensation product.

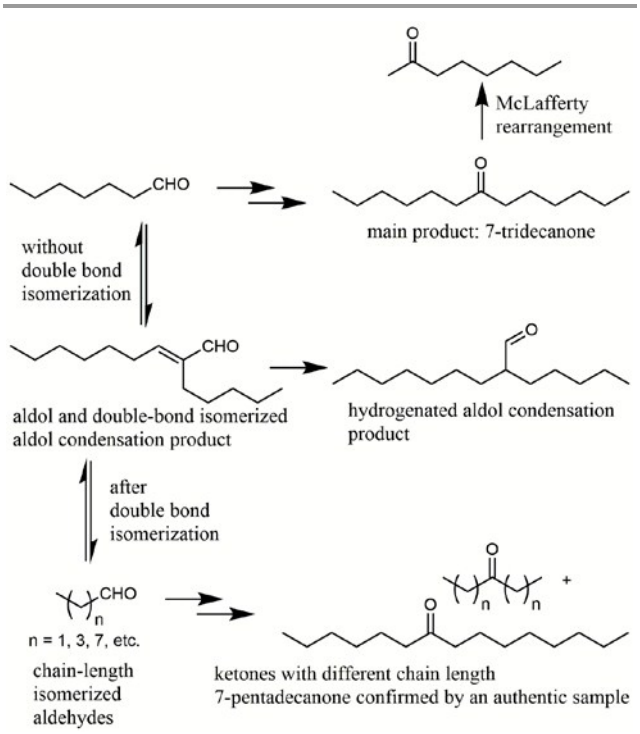

Scheme 5. Complete reaction network for the transformation of heptanal over cerium oxide. During the ketonization reaction heptanal is oxidized into heptanoic acid which is subsequently transformed into the symmetrical ketone 7-tridecanone. The latter ketone can undergo McLafferty rearrangement causing a fragmentation of the ketone and formation of 2-octanone. In parallel to the ketonization pathway the aldehyde is in equilibrium with its aldol condensation product. The latter can undergo double bond isomerization and hydrogenation. When the hydrogenation occurs the saturated aldehyde is produced. Isomerized aldol condensation products are observed in the product mixture (detected by GC-MS). However, they can also react back to the aldehyde stage and produce aldehydes with different chain length. The ketonization of these aldehydes provides ketones with different chain length or with a different carbonyl group position.

Alternatively, a reduced product may be obtained by Cannizzaro disproportionation of the aldol condensation product, an allylic alcohol together with the corresponding acid (Scheme 4, upper pathway). However, when the allyl alcohol was produced by $NaBH_4$ reduction or the unsaturated acid by autoxidation the corresponding compounds were not detected in the product mixture. This excludes reduction by occurrence of the Cannizzaro disproportionation and confirms unequivocally the double bond reduction of the aldol condensation product under the present reaction conditions.

Aldehydes might also be decarbonylated, forming an alkane (or arene) and carbon monoxide. Although in general metal catalysis is required for this reaction,[35–38] the high temperature employed in the present case may also facilitate it. Therefore, the corresponding product hexane was monitored. From Figure S10 it can be seen that the yield of this product was always below 2% yield. Therefore, it can be concluded that decarbonylation is not an important reaction pathway for the reaction of heptanal over CeO_2.

The complete reaction network can be established as depicted in Scheme 5. In general, the selectivity towards aldol condensation products in the presence of water is low (<5%, see e.g. Table 2, entries 1 to 4), but isomerized aldol condensation products are observed in higher selectivity when the aldol condensation product is fed directly. Ketones derived from fragmentation and chain length isomerization are avoided especially with small crystal size material (<10 nm). Here the selectivity towards these products is limited to selectivities of 10% (Table 2, entries 1 to 3).

The ketonization and hydrodeoxygenation cascade

One particular application of the ketonization of aldehydes is the up-grading of biomass-derived mixtures to bio-fuels. Thereby, complete hydrodeoxygenation is desired. To achieve this an additional reaction step has to be carried out subsequently to convert the ketone into an alcohol, then into an olefin and, last, into the alkane. This cascade reaction has been established starting from carboxylic acids.[39–41] However, when employing aldehydes the reaction possesses a special attraction since during the reaction of the aldehyde two equivalents of hydrogen are produced per molecule of ketone and this is exactly the amount required to convert the ketone into the alkane. Even more, in the hydrodeoxygenation one molecule of water is produced which replaces the one consumed for the oxidation of the aldehydes. In summary, balancing the overall equation of all five reaction steps two aldehyde molecules are converted into a linear alkane with 2n–1 carbon atoms and one molecule of carbon dioxide (Scheme 6).

For the hydrodeoxygenation, literature conditions were selected i.e. alumina supported platinum as catalyst and a reaction temperature of 300 °C. In preliminary tests it was found that the reaction at atmospheric pressure, applying either a nitrogen or a hydrogen flow, the conversion of the ketone was not complete. Therefore, the reaction was carried out applying a 2·10^6 Pa hydrogen pressure. Under these conditions it can be seen that the conversion of the ketone was

View Article Online
DOI: 10.1039/C6GC03511F

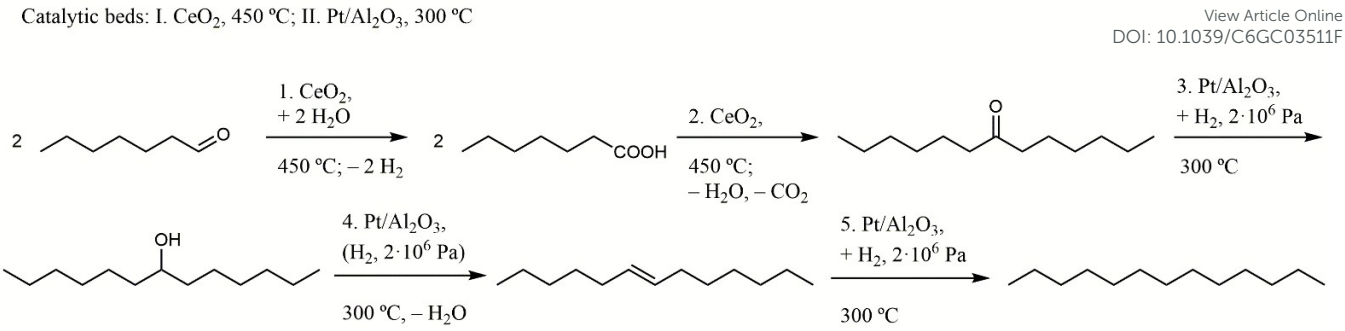

Scheme 6. Cascade reaction from heptanal to tridecane. In the first step the aldehyde hydrate is dehydrogenated over CeO_2 at 450 °C, i.e. per two aldehyde molecules two water molecules are consumed and two hydrogen molecules and two carboxylic acids produced. In the second step two molecules of heptanoic acid are joined into 7-tridecanone, co-producing one molecule each of water and carbon dioxide. In the third step, changing to Pt/Al_2O_3 as catalyst and applying a hydrogen pressure of $2{\cdot}10^6$ Pa and a temperature of 300 °C, the ketone is reduced into the corresponding alcohol. In the fourth step the alcohol is dehydrated under the same reaction conditions. Finally, in the fifth step the olefin is hydrogenated into linear tridecane.

higher than 95% (Figure 11). Tridecane, the linear alkane produced from 7-tridecanone, was obtained in 60% yield and an additional 30% of other alkanes. The latter were derived from the hydrodeoxygenation of other ketones (e.g. C_8H_{18}, C_9H_{20}, $C_{11}H_{24}$, $C_{15}H_{32}$ and $C_{17}H_{36}$) and also of the aldol condensation-derived products ($C_{14}H_{30}$; Scheme 7). In addition, n-heptane was observed which was probably derived from non-ketonised heptanal. The exact composition of the alkane fraction is depicted in Figure S11.

The whole product mixture was evaluated as bio-fuel by simulated distillation. This is particularly interesting since heptanal is a residual aldehyde produced during the thermal treatment of methyl ricinoleate or castor oil.[42,43] The analysis indicated that almost 90% of the crude product mixture of the five-step cascade falls within the boiling point range of the diesel fraction (Figure 12). In addition, due to the high content of linear alkanes and mono-methylalkanes the quality as diesel fuel is excellent. Therefore, it can be concluded that combing the ketonization of aldehydes over cerium oxide with a subsequent hydrodeoxygenation step aldehydes can be transformed into a high quality diesel fuel. For this transformation (almost) no external hydrogen is consumed.

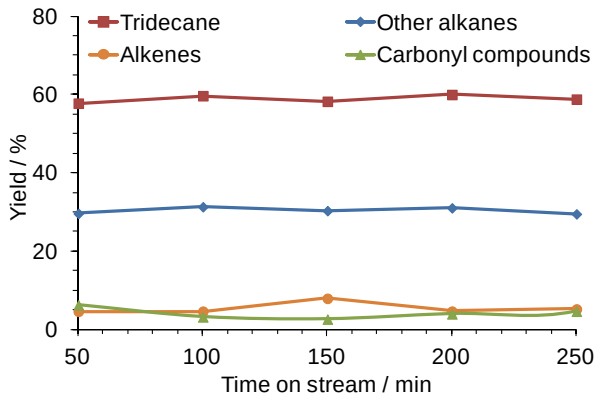

Figure 11. Product yields for the cascade reaction of heptanal to tridecane. Other alkanes are specified in Figure S11. Alkenes cover the whole range from C_6 to C_{20} and carbonyl compounds are mainly 7-tridecanone, 2-octanone and the aldol condensation product of heptanal. Reaction conditions: heptanal ketonization and 7-tridecanone hydrogenation reactions were carried out in two vertically connected fixed-bed reactors that were packed separately with 1 g of CeO_2-11nm and 1.5 g of Pt/Al_2O_3 and heated at 450°C and 300 °C respectively. Heptanal (5 mL, 0.1 mL min^{-1}) and water (0.638 mL, 0.013 mL min^{-1}) were fed separately into the reactor with heptanal : water molar ratio 1 : 1 under $2{\cdot}10^6$ Pa hydrogen pressure and a flow of 220 mL min^{-1}. The mass balance for the organic phase was approximately 95% for every reaction (calculated with respect to the theoretical yield, subtracting the weight of one molecule of carbon dioxide).

Conclusions

It has been shown that cerium oxide with a small crystal size (<15 nm) is an active and selective catalyst for the ketonization of aldehydes. In contrast to zirconium oxide, the catalytic activity for the competing aldol condensation is low which on one hand allows to obtain higher selectivity but which on the other hand converts water into a scarce compound on the catalyst surface. Since water is consumed during the reaction, it has to be co-fed to maintain catalytic activity.

From the distribution pattern of the ketone by-products observed it can be concluded that cerium oxide catalyses in parallel an aldehyde chain length isomerization. As a

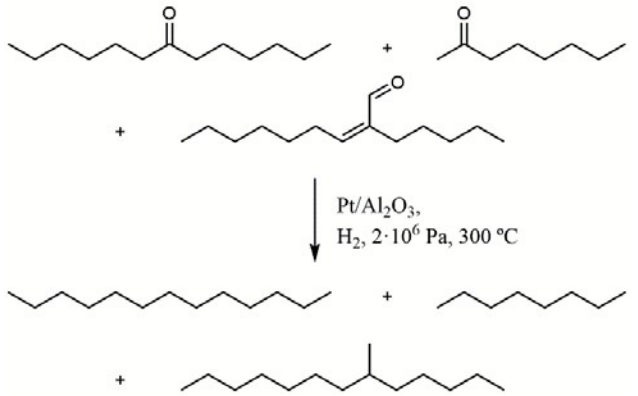

Scheme 7. Hydrodeoxygenation of the main products: 7-tridecanone is transformed into tridecane, 2-octanone into octane and 2-pentyl-2-nonenal into 6-methyltridecane.

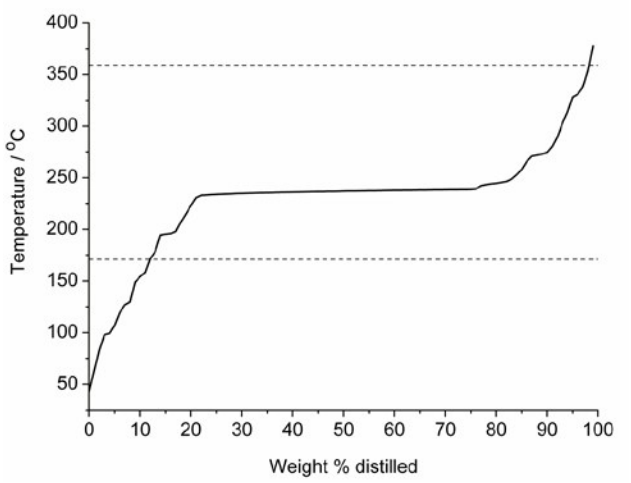

Figure 12. Simulated distillation of the product mixture of the reactions of heptanal over CeO_2-11nm to produce 7-tridecanone as main compound, followed by hydrogenation over Pt/Al_2O_3 to produce tridecane and other alkanes. Horizontal lines indicate temperature limits for the boiling point ranges of diesel fuels (171-359 °C).

consequence, ketones with different chain length were observed, including isomers with more carbon atoms than the one expected as product with 2n–1 carbon atoms. In addition, hydride transfer to double bonds activated by carbonyl groups in conjugation has been detected.

The ketonization of aldehydes over cerium oxide can be combined with a hydrodeoxygenation. Thereby, a cascade reaction is designed consisting of five subsequent steps occurring in two catalytic beds. With this concept, the hydrogen produced during the aldehyde oxidation can be consumed during the hydrodeoxygenation. In the balanced overall reaction equation two aldehyde molecules are transformed into a linear alkane on the expense of one carbon dioxide molecules as co-product. When the reaction is carried out with heptanal, the latter is transformed into a very good quality diesel fraction with almost 90% selectivity.

Acknowledgements

The authors thank MINECO (CTQ2015-67591-P and Severo Ochoa program, SEV-2012-0267) and Generalitat Valenciana (PROMETEO II/2013/011 Project) for funding this work. L.M.O. is grateful to the COLCIENCIAS institute for a Francisco-Jose-de-Caldas (512/2010) doctoral fellowship. Assistance and advice received from the Electron Microscopy Service at the Universitat Politècnica de València is also acknowledged.

Notes and references

1 J. Q. Bond, D. M. Alonso, D. Wang, R. M. West and J. A. Dumesic, *Science*, 2010, **327**, 1110–1114.

2 B. G. Harvey and H. A. Meylemans, *Green Chem.*, 2014, **16**, 770–776.

3 R. L. Wingad, E. J. E. Bergström, M. Everett, K. J. Pellow and D. F. Wass, *Chem. Commun.*, 2016, **52**, 5202–5204.

4 D. Gabriëls, W. Y. Hernández, B. F. Sels, P. Van Der Voort and A. Verberckmoes, *Catal. Sci. Technol.*, 2015, **5**, 3876–3902.

5 G. W. Huber, J. N. Chheda, C. J. Barrett and J. A. Dumesic, *Science*, 2005, **308**, 1446–1450.

6 S. De, B. Saha and R. Luque, *Bioresour. Technol.*, 2015, **178**, 108–118.

7 H. R. Beller, E.-B. Goh and J. D. Keasling, *Appl. Environ. Microbiol.*, 2010, **76**, 1212–1223.

8 G. Kumar, J. L. Johnson and P. A. Frantom, *Biochemistry*, 2016, **55**, 1863–1872.

9 I. L. Simakova and D. Y. Murzin, *J. Energy Chem.*, 2016, **25**, 208–224.

10 A. Corma Canos, S. Iborra and A. Velty, *Chem. Rev.*, 2007, **107**, 2411–2502.

11 G. W. Huber and A. Corma, *Angew. Chemie - Int. Ed.*, 2007, **46**, 7184–7201.

12 D. Mohan, C. U. Pittman and P. H. Steele, *Energy and Fuels*, 2006, 20, 848–889.

13 Q. Zhang, J. Chang, T. Wang and Y. Xu, *Energy Convers. Manag.*, 2007, **48**, 87–92.

14 A. Demirbas, *Appl. Energy*, 2011, 88, 17–28.

15 D. K. Shen and S. Gu, *Bioresour. Technol.*, 2009, **100**, 6496–6504.

16 L. M. Orozco, M. Renz and A. Corma, *ChemSusChem*, 2016, **9**, 2430–2442.

17 A. Pulido, B. Oliver-Tomas, M. Renz, M. Boronat and A. Corma, *ChemSusChem*, 2013, **6**, 141–151.

18 A. Gangadharan, M. Shen, T. Sooknoi, D. E. Resasco and R. G. Mallinson, *Appl. Catal. A Gen.*, 2010, **385**, 80–91.

19 M. B. Smith and J. March, *March's Advanced Organic Chemistry: Reactions, Mechanisms, and Structure*, John Wiley and Sons, John Wiley & Sons, Inc., 7th edn., 2013.

20 H.-X. Mai, L.-D. Sun, Y.-W. Zhang, R. Si, W. Feng, H.-P. Zhang, H.-C. Liu and C.-H. Yan, *J. Phys. Chem. B*, 2005, **109**, 24380–24385.

21 J. C. Conesa, *Surf. Sci.*, 1995, **339**, 337–352.

22 A. Badri, C. Binet and J. Lavalley, *J. Chem. Soc., Faraday Trans.*, 1996, **92**, 4669–4673.

23 H. Idriss, C. Diagne, J. P. Hindermann, A. Kiennemann and M. A. Barteau, *J. Catal.*, 1995, 155, 219–237.

24 M. Kobune, S. Sato and R. Takahashi, *J. Mol. Catal. A Chem.*, 2008, **279**, 10–19.

25 R. S. Murthy, P. Patnaik, P. Sidheswaran and M. Jayamani, *J. Catal.*, 1988, **109**, 298–302.

26 Y. Kamimura, S. Sato, R. Takahashi, T. Sodesawa and T. Akashi, *Appl. Catal. A Gen.*, 2003, **252**, 399–410.

27 S. Sato, R. Takahashi, T. Sodesawa, K. Matsumoto and Y. Kamimura, *J. Catal.*, 1999, **184**, 180–188.

28 V. I. Komarewsky and J. R. Coley, *Adv. Catal.*, 1956, **8**, 207–217.

29 J. B. Claridge, M. L. H. Green, S. C. Tsang and A. P. E. York, *J. Chem. Soc. Faraday Trans.*, 1993, **89**, 1089–1094.

30 S. Ananthan, N. Venkatasubramanian and C. N. Pillai, *J. Catal.*, 1984, **89**, 489–497.

31 R. A. Hites and K. Biemann, *J. Am. Chem. Soc.*, 1972, **94**, 5772–5777.

View Article Online
DOI: 10.1039/C6GC03511F

32 D. M. Ohlmann, N. Tschauder, J.-P. Stockis, K. Gooßen, M. Dierker and L. J. Gooßen, *J. Am. Chem. Soc.*, 2012, **134**, 13716–13729.
33 G. Vilé, B. Bridier, J. Wichert and J. Pérez-Ramírez, *Angew. Chemie - Int. Ed.*, 2012, **51**, 8620–8623.
34 J. Carrasco, G. Vilé, D. Fernández-Torre, R. Pérez, J. Pérez-Ramírez and M. V. Ganduglia-Pirovano, *J. Phys. Chem. C*, 2014, **118**, 5352–5360.
35 E. I. Gürbüz, D. D. Hibbitts and E. Iglesia, *J. Am. Chem. Soc.*, 2015, **137**, 11984–11995.
36 P. Malcho, E. J. Garcia-Suarez, U. V. Mentzel, C. Engelbrekt and A. Riisager, *Dalton Trans.*, 2014, **43**, 17230–17235.
37 A. Modak, A. Deb, T. Patra, S. Rana, S. Maity and D. Maiti, *Chem. Commun.*, 2012, **48**, 4253–4255.
38 S. R. Yenumala, S. K. Maity and D. Shee, *React. Kinet. Mech. Catal.*, 2016, 1–20.
39 J. C. Serrano-Ruiz, D. Wang and J. A. Dumesic, *Green Chem.*, 2010, **12**, 574–577.
40 A. Corma, M. Renz and C. Schaverien, *ChemSusChem*, 2008, **1**, 739–741.
41 A. Corma, B. Oliver-Tomas, M. Renz and I. L. Simakova, *J. Mol. Catal. A Chem.*, 2014, **388–389**, 116–122.
42 T. J. Farmer and M. Mascal, in *Introduction to Chemicals from Biomass*, John Wiley & Sons, Ltd, 2015, pp. 89–155.
43 H.-B. Hu, K.-W. Park, Y.-M. Kim, J.-S. Hong, W.-H. Kim, B.-K. Hur and J.-W. Yang, *J. Ind. Eng. Chem.*, 2000, **6**, 238–241.
44 A. L. Patterson, *Phys. Rev.*, 1939, **56**, 978–982.
45 G. da Silva and J. W. Bozzelli, *J. Phys. Chem. A*, 2006, **110**, 13058–13067.
46 S. P. Verevkin, *J. Chem. Eng. Data*, 2000, **45**, 953–960.
47 K. G. Joback and R. C. Reid, *Chem. Eng. Commun.*, 1987, **57**, 233–243.

View Article Online
DOI: 10.1039/C6GC03511F

Atom-efficient transformation of two aldehyde molecules into a linear alkane on the expense of one carbon dioxide molecule.